Evaluation of Plume Divergence and Facility Effects on Far-Field Faraday Probe Current Density Profiles

IEPC-2009-030

Presented at the 31st International Electric Propulsion Conference,
University of Michigan • Ann Arbor, Michigan • USA
September 20 – 24, 2009

Daniel L. Brown[1]
Air Force Research Laboratory, Edwards AFB, CA, 93524, USA

and

Alec D. Gallimore[2]
University of Michigan, Ann Arbor, MI, 48109, USA

Abstract: A Faraday probe with three concentric rings was designed and fabricated to assess the effects of gap width and probe geometry in a systematic study of the Hall thruster plume. The nested Faraday probe consisted of two concentric collector rings and an outer guard ring, which enabled simultaneous current density measurements on the inner and outer collector. Two versions of the outer collector were fabricated to create 0.5 mm or 1.5 mm gaps between the rings. Current density distribution of a Hall thruster ion source were studied at 8, 12, 16, and 20 thruster diameters downstream of the exit plane with four probe configurations at background pressures of $3x10^{-6}$, $1x10^{-5}$, and $3x10^{-5}$ torr. Several correction factors are proposed to account for the effective probe collection area and systematic measurement error associated with measuring an annular device as a point source. These corrections enable the investigation of beam expansion and ion migration from the central core, and result in a highly accurate estimate of divergence in the Hall thruster plume. Application of the correction factors and characterization of facility effects are shown to decrease the calculated beam current by 10-20% compared to conventional analysis and reduce measurement uncertainty to ±3%.

[1] Research Scientist, Spacecraft Branch, Propulsion Directorate, AFRL/RZSS, Daniel.Brown@edwards.af.mil.
[2] Professor, Department of Aerospace Engineering, Associate Dean, Horace H. Rackham School of Graduate Studies, Director, Plasmadynamics and Electric Propulsion Laboratory, Alec.Gallimore@umich.edu.

Nomenclature

$A_{0,1,2}$	second order polynomial coefficients	[-]
A_C	projected cross-sectional area of the Faraday probe collector	[m^2]
$\overline{A}_C$	side-wall surface area of the Faraday probe collector	[m^2]
$A_{Effective}$	corrected cross-sectional collection area of the Faraday probe collector and gap	[m^2]
A_{Gap}	projected cross-sectional area of the Faraday probe gap	[m^2]
$\overline{A}_{GR}$	side-wall surface area of the Faraday probe guard ring	[m^2]
g	gap width between the Faraday probe collector and guard ring	[m]
h_C	height of the Faraday probe collector	[m]
h_{GR}	height of the Faraday probe guard ring	[m]
I_{Axial}	axial component of ion beam current parallel to thruster centerline	[A]
I_{Beam}	integrated ion beam current	[A]
I_d	anode discharge current	[A]
$I[\theta]$	collected Faraday probe current at angular position θ	[A]
$J[\theta]$	current density in the plume at angular position θ	[A/m^2]
p	corrected facility background pressure for working gas	[torr]
p_b	vacuum facility base pressure for air	[torr]
p_i	background pressure measured by an ionization gauge	[torr]
R	downstream measurement distance from the axis of rotation	[m]
R_C	outer radius of the Faraday probe collector	[m]
R_{CL}	channel centerline radius of the thruster	[m]
R_{GR}	inner radius of the Faraday probe guard ring	[m]
R_L, R_R	downstream distance from the left or right ion point source to the Faraday probe	[m]
α_A	ion angle of divergence relative to channel centerline	[rad]
α_L, α_R	angle of incidence from the left and right point sources to the Faraday probe	[rad]
θ	angular position, horizontal plane in spherical coordinate system	[rad]
κ_A	Faraday probe correction accounting for ion angle of incidence to the probe	[-]
κ_D	Faraday probe correction accounting for probe distance to channel centerline	[-]
κ_G	Faraday probe area correction accounting for ion collection in the gap	[m^2]
λ	plume momentum divergence half-angle, λ=0 on thrust axis	[rad]

Operations

$[R, R_{CL}, \theta]$	parameter measured or calculated as a function of R, R_{CL}, and/or θ
$< >_{mv}$	momentum-weighted average quantity in the plume, at constant R ($0<\theta<\pi$)
$< >_J$	current-weighted average quantity in the plume, at constant R ($0<\theta<\pi$)

I. Introduction

ACCURATE assessment of current density in the Hall thruster plume is required to study ion beam divergence and to quantify the fraction of cathode electron current to the anode. Faraday probe current density measurements are typically used for qualitative evaluation of the plume profile as opposed to quantitative assessment, since calculations of total ion beam current are often greater than the thruster discharge current. In addition, beam divergence is artificially increased with distance from the exit plane due to particle scattering from the central core to the wings of the plume. These over-predictions are exacerbated at high background pressure and large angles from thruster centerline, and are attributed to facility effects.[1]

This research was initiated to reduce the measurement uncertainty of Faraday probes and enable accurate calculations of ion beam current and plume divergence. A nested Faraday probe was designed and fabricated to systematically characterize facility effects on ion current density profiles in a Hall thruster plume over a wide range of downstream distances and facility background pressure. Correction factors are introduced to account for probe geometry and spatial effects associated with the measurement coordinate system. The ion current density distributions are studied to advance understanding of facility effects on the Hall thruster plume, and thereby improve comparisons of ground-based experimental measurements with simulations of the on-orbit plume. The analytical and experimental techniques minimize facility effects and lead to a list of recommendations for high-accuracy Faraday probe measurements.

II. Past Investigations

A number of studies have investigated the effects of elevated background pressure, compared nude Faraday probe designs, and evaluated design modifications in order to minimize uncertainty due to charge exchange (CEX) collisions in the plume. Measurements of several Hall thruster designs by Manzella and Sankovic[2] found high background pressure increased ion current density on the wings, while the central core remained largely unaffected. Discharge current increased linearly with increasing pressure, which was attributed to neutral xenon ingested into the discharge channel. Ingested propellant was ionized and accelerated to create additional ion beam current in the plume and electron current to the anode, thereby increasing discharge current. The escalation of current density at high angles off thruster centerline axis was due to CEX collisions between fast moving ions and slow moving xenon from the background gas. The resulting slow moving ions are scattered from the central core to the outer wings.

Past investigations at the Plasmadynamics and Electric Propulsion Laboratory (PEPL) evaluated Faraday probe design and facility background pressure on collected ion current. A comparison of two nude Faraday probe designs concluded the differences in measured current density were due to probe design and dissimilar secondary electron emission (SEE) properties of the collectors.[3,4] For tests using the P5 Hall thruster at several operating conditions, increasing facility backpressure increased the current density on the wings. The lower current, 4.3-A case showed the current distribution in the central core was unaffected by backpressure, similar to results by Manzella and Sankovic.[2] However, the higher current 10-A case exhibited minor increases in the central core current density, and was attributed to ionization and acceleration of the background neutrals near the exit plane. These trends are consistent with far-field Faraday probe measurements using the SPT-140.[5]

Plasma potential in the region surrounding a nude Faraday probe has been measured to study the possibility of probe bias voltage acting as a point source potential sink, and thereby attracting low energy CEX ions.[6] Langmuir probe measurements near a nude Faraday probe determined the plasma potential varied by less than 3-V within 20-mm of the probe. It was concluded that CEX ions had a negligible attraction to the probe bias potential, and the random flux of low energy ions was insufficient to explain the increased current density at high background pressure and large off-axis angles. This conclusion was consistent with computational modeling of the ion flow around an axisymmetric Faraday probe. A hybrid-PIC model simulated the collected current for off-axis conditions present in a low-power HET plume, and found errors due to sheath expansion were minimal.[7]

To mitigate the collection of low energy ions created in CEX collisions, numerous filtering mechanisms have been investigated. One approach is to attach a collimator to the entrance of a nude Faraday probe to filter low energy ions that are created by CEX collisions in the plume.[8,9] Ions created by CEX collisions near the exit plane and directed to the probe are still collected. The CEX ion population resulting from collisions with the anode and cathode thruster neutrals is present on orbit, but CEX collisions with facility neutrals and the ions attributed to entrainment of facility neutral flow may also be collected.

Further efforts utilized a magnetic field to filter low energy CEX ions. A study by Rovey, *et al.*[10] compared results from a magnetically filtered Faraday probe, a boxed Faraday probe, and a nude Faraday probe to separately assess the effect of the magnetic filter and the boxed collimator that houses the filter. Similar to past results, the nude Faraday probe exhibited increased beam current and larger current density on the wings with increasing background pressure. The magnetically filtered and boxed Faraday probes resulted in decreased beam current and diminished current density on the wings with increasing background pressure. The central core measured by all three probes was unaffected by increased chamber pressure. These findings indicate the boxed collimator and magnetic filtering decrease low energy CEX ions collected by the Faraday probe. The downside of these approaches is that they do not selectively filter facility effects from the ionization of thruster neutrals downstream of the primary acceleration zone.

A different method for discerning CEX processes in the plume was demonstrated by de Grys, *et al.*[8] and more recently by Azziz[11], who compared Faraday probe measurements at individual locations in the plume at several background pressures and extrapolated the current density to vacuum conditions. This approach is a more advanced technique to experimentally assess CEX facility effects throughout the plume, and enables a more accurate estimation of the on-orbit ion current density distribution.

A comprehensive investigation of nude Faraday probe design and analytical technique was conducted at AFRL with a nested Faraday probe.[12] Enhanced understanding of Faraday probe ion current collection led to development of a gap correction factor that reduced the integrated ion beam current by ~20%. The corrected plume properties were in line with expected values of ion beam current based on Hall thruster performance and discharge properties. A key discovery was the ability to predict the amount of additional ion current on the collector side walls. The study indicated conventional Faraday probe designs with a ceramic base are more suitable for characterization of facility

effects and current density mapping with a wide range of Debye lengths in the plume. This gap correction is detailed in Section IV.

III. Experimental Apparatus

A. Facility and Measurement Positioning System

The investigation was conducted in Chamber 1 at AFRL/RZSS using a low-power Hall thruster ion source. Chamber 1 at AFRL is a stainless steel, cylindrical vacuum chamber 2.4-m in diameter and 4-m in length with a maximum xenon pumping speed of 50,000 l/s. The thruster was located along the centerline of the chamber and fired towards the cryopanels at the opposing end. Prior to Faraday probe data collection, the thruster was fired for over 1-hour after initial start-up. Thruster telemetry was monitored during Faraday probe sweeps, and exhibited negligible deviation from steady-state operation.

An MKS Instruments cold cathode ionization gauge was located on the chamber ceiling above the thruster centerline approximately 1-meter downstream of the exit plane. Background pressure was corrected using Eq. (1) with a xenon correction factor of 2.87 and the facility base pressure (p_b) of air, which was conservatively estimated at $p_b \approx 1\text{x}10^{-7}$ torr. Chamber background pressure was increased by injecting xenon through an auxiliary flow line located approximately 1-meter downstream of the thruster exit plane. Injected flow of 9, 29, and 127-sccm corresponded to a corrected xenon background pressure of $3.2\text{x}10^{-6}$, $1.1\text{x}10^{-5}$, and $3.5\text{x}10^{-5}$ torr, respectively.

$$p = \frac{p_i - p_b}{2.87} + p_b \tag{1}$$

The Faraday probe positioning system consisted of a translation stage for control of measurement radius and a rotation stage, which was centered beneath the exit plane on thruster centerline. In Fig. 1, one end of the translation stage is shown mounted on top of the rotation stage, enabling current density scans from 0° to 180° at constant radius up to 60-cm from the axis of rotation at the exit plane. The Faraday probe and laboratory thruster were mounted more than 50-cm above the rotation and translation stages. A National Instruments MID-7604/7602 Power Drive interfaced with the rotation and translation stages, and data acquisition was controlled through LabView.

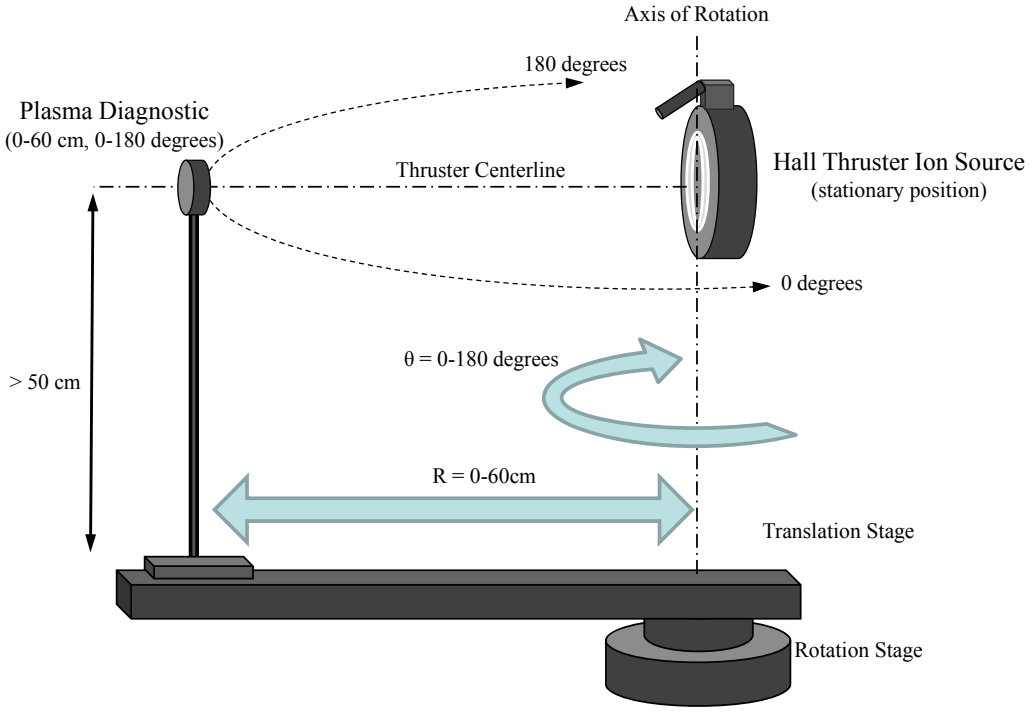

Figure 1. Diagnostic positioning system in Chamber 1 with R,θ-coordinate axis control.

B. Faraday Probe Design

Faraday probes measure the ion current collected by a negatively biased surface. Equal bias potential is applied to the collector and guard ring to create a flat, uniform sheath across the collector surface that repels electrons. A Faraday probe with three concentric rings was designed and fabricated to assess the effect of gap width and probe geometry in a systematic study of the Hall thruster plume. The nested Faraday probe consisted of two concentric collector rings and an outer guard ring, which enabled simultaneous current density measurements on the inner and outer collector. Two versions of the outer collector, also referred to as Collector 2, were fabricated to create gaps of 0.5-mm and 1.5-mm between the rings. For either version of Collector 2, the gap between Collector 1 and Collector 2 is always the same as the gap between Collector 2 and the guard ring. The collectors and guard ring are seated within a boron nitride shell and are different heights to form a highly concentric probe with uniform gap width, as shown in the diagram in Fig. 2. Probe dimensions are listed in Table 1.

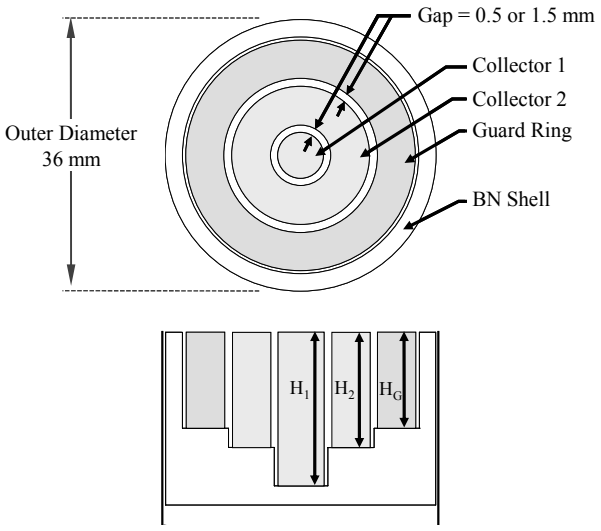

Figure 2. Top-view and cross-sectional diagrams of the AFRL nested Faraday probe.

Table 1. Nested Faraday probe dimensions

	Collector 1	Collector 2		Guard Ring
		0.5 mm Gap	1.5 mm Gap	
Inner Diameter [mm]	-	7.06	9.16	20.27
Outer Diameter [mm]	6.11	18.91	17.06	29.93
Height [mm]	15.58	13.75	13.76	10.22
Collector 1 – 2 Gap [mm]	-	0.48	1.53	-
Collector 2 – Guard Ring Gap [mm]	-	0.68	1.61	-

Unpublished experimental estimates of the electron temperature and ion number density in the plume of this low-power Hall thruster ion source indicated the Debye length ranged from 0.05 mm to ~1 mm throughout the plume from 8 to 20 thruster diameters downstream of the exit plane. Thus, the 0.5 mm gap configuration is less than or equal to 10 Debye lengths for all locations studied with the nested Faraday probe. The 1.5 mm gap configuration is greater than 10 Debye lengths, and was oversized to highlight the effects of a gap width greater than the $10\lambda_D$ design criteria.

There are four probe collection geometries that may be studied using the nested Faraday probe. These configurations are shown in Fig. 3 and referred to as:

1. Configuration 1 – Current to Collector 1 with a 0.5 mm gap
2. Configuration 2 – Combined current to Collector 1 and 2 with a 0.5 mm gap
3. Configuration 3 – Current to Collector 1 with a 1.5 mm gap
4. Configuration 4 – Combined current to Collector 1 and 2 with a 1.5 mm gap

For either the 0.5 mm or 1.5 mm gap configuration, the current collected by Collector 1 is compared to the combined current on Collector 1 and Collector 2 (termed Collector 1+2). Adding the collected current isolated effects caused by the inner gap to Collector 1 from effects caused by the outer gap to Collector 1+2. If the collected current were not added in this manner, Collector 2 may be influenced by effects between the inner gap (Collector 1 with Collector 2) and the outer gap (Collector 2 with the guard ring). This analysis allowed comparison of simultaneous measurements to different collection cross-sections with the same gap width.

The collectors were machined from arc-cast low-carbon grade 365 molybdenum, and the guard ring is grade 360 molybdenum. Differences in secondary electron emission between the collectors and guard ring due to electrode material and surface roughness should be minimal. Collection surfaces were machined to a standard 32 μ" AA finish. A 20-cm long stainless steel tube houses the boron nitride (BN) shell and probe leads. This stainless steel housing extends to the probe face and is grounded to create known boundary conditions for probe simulations. Trials with the SS housing allowed to float caused no change in collected current. All subsequent measurements were taken with the SS housing connected to chamber ground.

Collected current on both collectors and the guard ring were measured with an Agilent 34970A Data Acquisition Switch Unit. An Agilent E3631A Triple Output DC power supply was used to bias the collectors and guard ring to the same potential. The schematic in Fig. 4 shows the circuit diagram for equal bias potential on all rings. The nested Faraday probe operation was characterized with variations in probe bias potential over a range of angular positions and downstream distances at several facility background pressures. A bias potential of -20 V with respect to facility ground was beyond the ion current saturation limit in all cases. Current density in the plume was measured in 2° increments from 0° to 180° at 8, 12, 16, and 20 thruster diameters downstream of the Hall thruster exit plane.

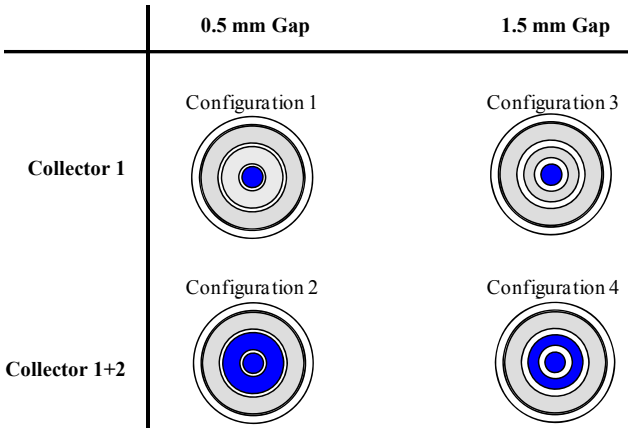

Figure 3. Top view of the four collection area configurations of the nested Faraday probe. Regions of blue are the current collecting surfaces orthogonal to the beam.

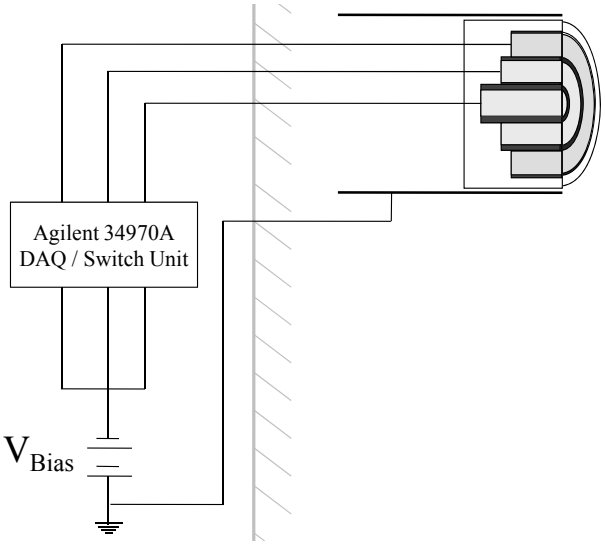

Figure 4. Electrical diagram of the nested Faraday probe power electronics and DAQ system.

IV. Faraday Probe Correction Factors

A. Gap Correction Factor for the Effective Probe Collection Area

Extensive experimental evidence has shown that Faraday probe measurements typically overestimate ion beam current in the Hall thruster plume. This phenomenon is typically attributed to additional ion current from CEX facility effects, but has been shown to result from under-prediction of the effective probe collection area. In conventional nude Faraday probe design and analysis, the collection area is calculated as the geometric surface area of the collector ($A_C = \pi R_C^2$). Studies with the nested Faraday probe demonstrated that ions within the gap between the collector and guard ring contribute to the collected probe current, and may cause erroneously high ion current density in the plume if the geometric surface area of the collector is assumed.[12]

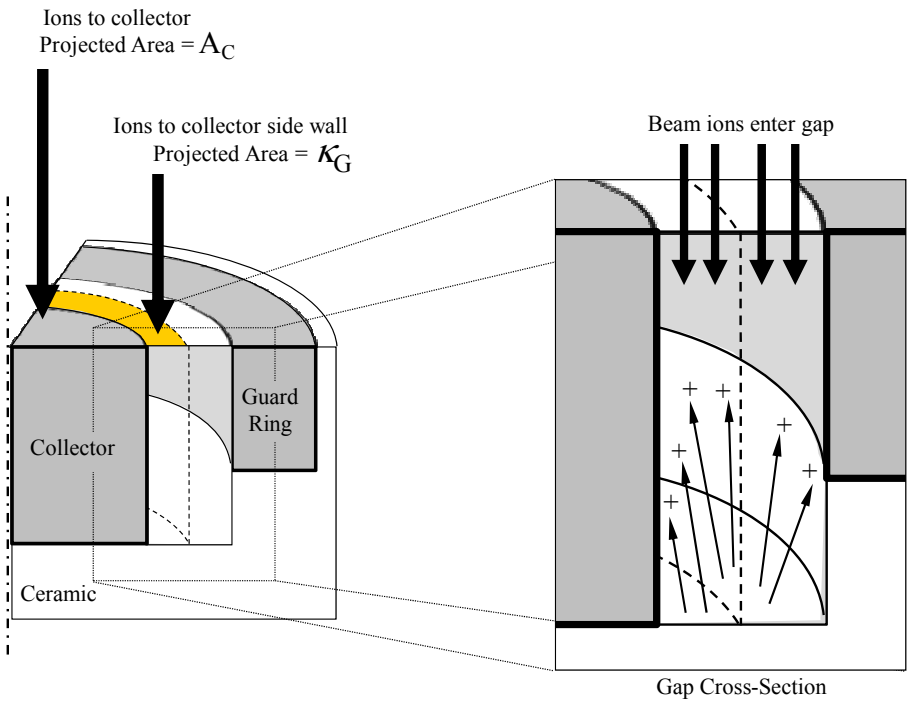

Figure 5. Illustration of ions collected by the side walls of the nested Faraday probe and the increase in projected collection area.

In this hypothesis, high energy beam ions entering the gap volume impact the ceramic base of the nested Faraday probe, and the resulting low energy ions are collected by the walls of the negatively biased electrodes. A fraction of this current is collected on the side walls of the collector, thereby increasing the collected ion current and causing an overestimate of the current density. This effect is shown in Fig. 5. The orange region illustrates the increase in the projected collection area to account for ion current to the collector side wall.

To correct for this increase in the effective probe collection area, a Faraday probe gap correction factor, κ_G, was developed to account for differences in collector diameter and gap width. This correction factor partitions the current collected in the gap volume based on the ratio of the side wall surface areas. The geometric probe collection area is increased according to Eq. (2) to account for ions entering the gap volume that are collected by the collector side wall. The gap correction factor, κ_G, is defined in Eq. (3) as a function of the probe geometry shown in Fig. 6.

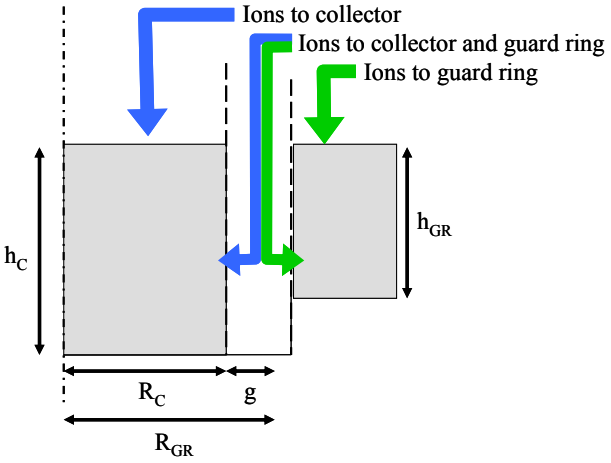

Figure 6. Diagram of the nude Faraday probe collector (outer radius R_c, height h_C), guard ring (inner radius R_{GR}, height h_{GR}) and gap width (g).

$$A_{Effective} = \pi R_C^{\,2} + \kappa_G \tag{2}$$

$$\kappa_G = A_{Gap}\left(\frac{\overline{A}_C}{\overline{A}_C + \overline{A}_{GR}}\right) = \pi\left(R_{GR}^{\,2} - R_C^{\,2}\right)\left(\frac{2\pi R_C h_C}{2\pi R_C h_C + 2\pi R_{GR} h_{GR}}\right) \tag{3}$$

Based on this hypothesis, the effective probe collection area would show the greatest increase for designs with a large gap width and a large collector side wall surface area. The projected area of a 5-10 Debye length gap width may collect a significant fraction of the measured ion current, especially for a probe with a small collector diameter. It is important to note that the formulation in Eq. (3) is only applicable to conventional nude Faraday probes with a ceramic base in the gap volume. The ion collection of probe designs with a conductive base would be expected to behave differently. The gap correction factor increased the nested Faraday probe collection areas by approximately 10% to 55% to account for ion collection in the gap. The precision in total ion beam current measurements was within a 3% range for all nested Faraday probe configurations when the gap correction factor was applied., and the corrected plume properties were in line with expected values of ion beam current based on Hall thruster performance and discharge properties.[12]

B. Measurement Coordinate System Effects and Correction Factors

A detailed theoretical examination of the measurement coordinate geometry is necessary to isolate systematic trends due to facility effects in experimental measurements. The analysis is aimed at resolving the error caused by probe measurements with respect to a point source as opposed to the annular discharge geometry of a typical HET. Correction factors are developed for an axisymmetric system based on constant measurement radius from the probe axis of rotation, as illustrated in Fig. 1, where current density is integrated in a hemisphere around the point source. In the analysis, the thruster is modeled as two point ion sources located at the centerline of the discharge channel. Fig. 7 illustrates the probe distance and angular location with respect to the thruster centerline.

Two geometric corrections are analyzed. The first correction accounts for variations in probe angle with respect to the point sources, which will affect the current collection area. In a single point source analysis, where the ion point source is located at the probe axis of rotation, the probe face is perpendicular to the source as it is swept in a 180° arc. Modeling the thruster as two point sources changes this probe orientation, and the probe face is only perpendicular to the point sources at 0° and 180°. The ion angle of incidence to the probe face changes with angular position and distance, and decreases the effective probe collection area of beam ions. In addition, the ion angle of incidence at a given location is different for each point source. The angles of incidence are calculated for the left and right point sources as α_L and α_R, and are used to evaluate cosine losses in the probe collection area.

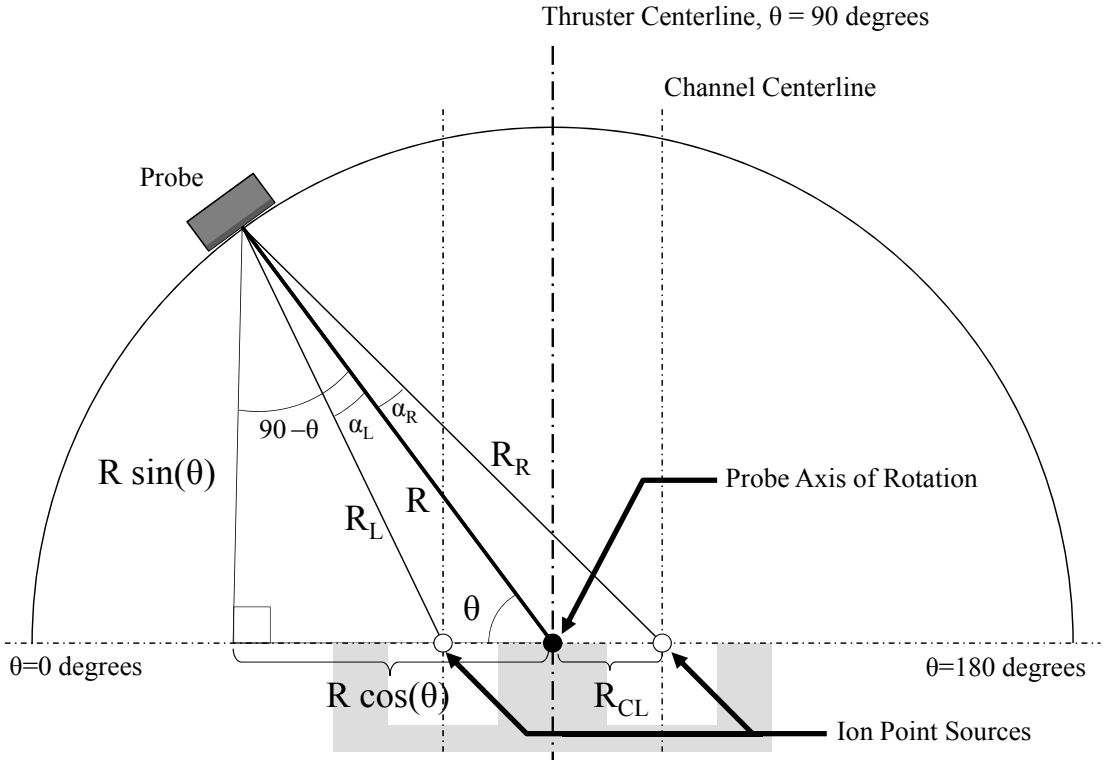

Figure 7. Coordinate system for probe distance and angular location in a two point source model.

The angles α_L and α_R are found using basic trigonometry and are formulated in Eq. (4) based on the geometry shown in Fig. 7. These effects are expressed in a generalized form based on the probe angular position θ, the probe distance from the axis of rotation R, and the channel centerline radius R_{CL}. The ratio of R/R_{CL} is incorporated to simplify the analysis and enable a more direct comparison between large and small thrusters.

$$\alpha_{L,R}\left[\theta, R, R_{CL}\right] = \pm\left(90 - \theta - \tan^{-1}\left(\frac{\cos(\theta) \mp \frac{R_{CL}}{R}}{\sin(\theta)}\right)\right) \tag{4}$$

The probe collection area is corrected for cosine losses with the area correction factor, κ_A, using the average of α_L and α_R in Eq. (5).

$$\kappa_A\left[\theta, R, R_{CL}\right] = \cos^2\left(\frac{\alpha_L + \alpha_R}{2}\right) \tag{5}$$

The second correction deals with the differences in path length from the left and right point sources to the probe, which introduces systematic error in the R^2 term in the axisymmetric plume integration. The probe distances from the left and right point source are characterized as R_L and R_R. Similar to the analysis of ion angle of incidence, the path length will vary with probe angular position and is dissimilar for each point source. The exception is on thruster centerline, where the distance from the probe to each point source is equal and greater than the measurement radius of rotation, R.

The lengths R_L and R_R are calculated with respect to the measurement distance, R, in Eq. (6). The distance correction factor, κ_D, is defined in Eq. (7) as a function of θ, R, and R_{CL}.

$$\frac{R_{L,R}\left[\theta, R, R_{CL}\right]}{R} = \sqrt{(\sin(\theta))^2 + \left(\cos(\theta) \mp \frac{R_{CL}}{R}\right)^2} \tag{6}$$

where,

$$\kappa_D\left[\theta, R, R_{CL}\right] = \left(\frac{1}{2}\left(\frac{R_L}{R} + \frac{R_R}{R}\right)\right)^2 \tag{7}$$

The effects of the area and distance correction factors are applied to all Faraday probe current density measurements. Therefore, the total ion beam current in this study is calculated using Eq. (8), which incorporates the corrections for measurement coordinate geometry and the collection of ions in the gap volume. For a Faraday probe scan at constant measurement radius R, the correction factors are a function of angular position, θ.

$$I_{Beam} = 2\pi R^2 \int_0^{\pi/2} \frac{I\left[\theta\right]}{A_C + \kappa_G}\left(\frac{\kappa_D\left[\theta, R, R_{CL}\right]}{\kappa_A\left[\theta, R, R_{CL}\right]}\right)\sin(\theta)\, d\theta \tag{8}$$

The spatial correction ratio (κ_D/κ_A) is displayed as a function of probe angular position in Fig. 8 for constant downstream measurement distance. The overall effect is to increase current density in the plume central core, which increases the integrated ion beam current. Variation in collection area due to ion angle of incidence decreases rapidly with downstream distance, and the approximation of a point source measurement improves. In Fig. 9, the correction on thruster centerline is shown as a function of downstream thruster diameters, calculated as $R/2R_{CL}$. The overall correction factor asymptotically approaches unity with downstream measurement distance, and is less than 1.02 for distances greater than 8 channel centerline diameters downstream (CCDD). Thus, including the spatial corrections minimizes a systematic source of error introduced from the hemispherical measurement system. All

current density traces and beam current calculations in this investigation will incorporate the spatial corrections for ion angle of incidence and measurement distance using the formulation in Eq. (8).

The corrections in probe collection area are only valid for beam ions originating near the exit plane. Charge exchange collisions downstream of the primary ionization region increase dispersion of ion velocity, and the correction is not relevant to this population. In addition, the analysis does not account for thruster channel width. This is of lesser concern, since minor variations in channel centerline radius will have a negligible effect on measurements taken beyond four thruster diameters.

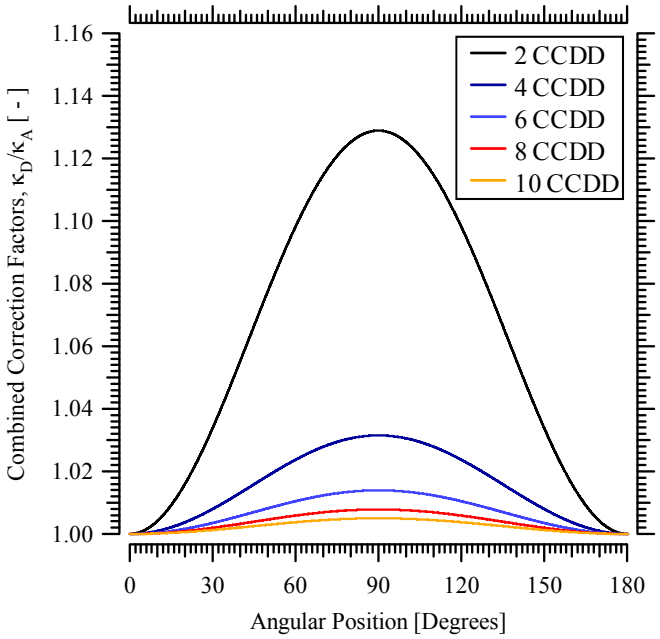

Figure 8. Combined effect of correction factors (κ_D/κ_A) accounting for the probe distance and angle with respect to the left and right ion point sources as a function of angular position with contours of constant $R/2R_{CL}$ = 2, 4, 6, 8, and 10 CCDD.

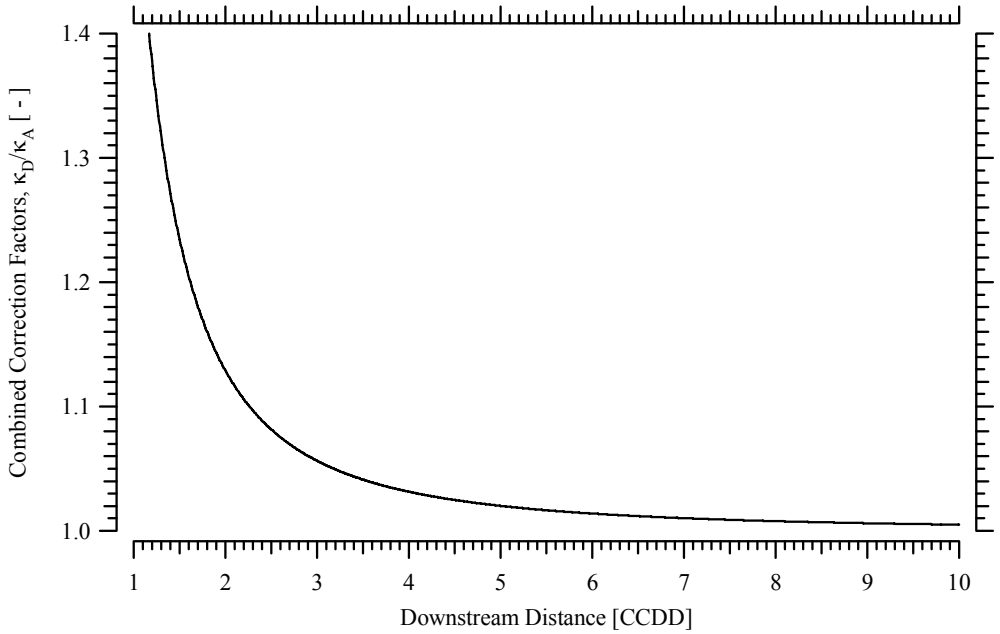

Figure 9. Combined effect of the correction factors (κ_D/κ_A) on channel centerline (θ=90°) as a function of downstream thruster diameters ($R/2R_{CL}$).

V. Analysis of Plume Scattering and Facility Effects

Corrections for measurement location and Faraday probe design were proposed to minimize systematic error, but facility effects also introduce a significant source of uncertainty that requires characterization of the thruster and chamber based on background pressure and operating conditions. Far-field Faraday probe measurements are generally prone to facility effects, and presumed to have relatively large uncertainty in the current density magnitude. Past investigations have examined the wings with variations in background pressure, and several methods have been developed to reduce collection of low energy facility CEX ions in the plume. Nevertheless, the integrated ion beam current from far-field measurements is typically larger than the value reported from near-field measurements, and is often greater than the thruster discharge current. In some cases, the thruster anode flow is modified to maintain a constant discharge current as pressure is adjusted. While this approach mitigates increased thrust due to the neutral ingestion of facility neutrals, it requires variation of thruster operating conditions and is not an ideal comparison between different background pressures. In this investigation of facility effects with the nested Faraday probe, the HET anode and cathode propellant flow rates are fixed. Background pressure is regulated through auxiliary injection of xenon.

Numerous experimental designs and analytical techniques have been used to minimize facility effects on far-field Faraday probe current density measurements. Experimental approaches include various types of filters to reduce collection of low energy CEX ions and measuring the ram current density using a backward facing Faraday probe. Current density profiles corrected with the ram current density are sensitive to background pressure, and the measurements are complicated by the wake surrounding the probe.[13] Filtration designs have proven to minimize CEX facility effects, but do not account for increased discharge current or ion beam current due to neutral propellant ingestion. In addition, a fraction of the filtered ions are present on-orbit due to CEX collisions with anode and cathode neutrals. This population should not be removed for an ideal evaluation of on-orbit plume divergence and current density distribution.

Analytical techniques include subtracting the ambient ion current density at $\theta=0°$ from the entire plume profile, or extrapolating the exponential region ($30°<\theta<50°$) of the ion current density to the outer periphery ($0°<\theta<30°$). While these approaches provide a simple alternative to the experimental methods, they are limited in determining the spatial influence of facility effects throughout the plume. Subtracting a finite current density from the profile based on the value at $\theta=0°$ is based on the assumption that collection of ambient tank ions is uniform throughout the plume. The exponential extrapolation is based on the spatial decay of beam ions on the edges of the primary beam, but removes features of the outer periphery that may arise due to CEX collisions near the thruster exit. Neither of these techniques accurately captures the angular distribution of low energy ions that would be present on orbit.

Studying the ion current density at each angular location in the plume as a function of background pressure enables a more accurate characterization of facility effects. Extrapolating the current density at discrete angular locations to vacuum conditions isolates effects arising from facility CEX ions and neutral ingestion. This technique is shown for Configuration 1 in Fig. 10 at 20 CCDD. Collected ion current is plotted in 10° increments as a function of facility background pressure. On thruster centerline at $\theta=90°$, the collected current increased linearly with background pressure. However, at ±10° from centerline the slope appears to transition and transforms to a slightly negative linear slope at ±20° and ±30° from thruster centerline. The reverse trend occurs at approximately ±40° and results in a positive linear slope on the periphery from ±60° to ±90° from thruster centerline.

These variations in the slope of the collected ion current with facility background pressure are plotted as a function of angular position in Fig. 11 at 8, 12, 16, and 20 CCDD. The transitions from positive to negative slope occur at approximately ±10° from thruster centerline for all downstream distances. Similarly, the transition from negative to positive slope occurs at approximately ±50° from thruster centerline for all downstream distances. Residuals show the degree of linearity at each angular location, and reveal that the transition at ±50° moves inwards toward the central core as downstream distance increases. This trend is indicative of the outward scattering of beam ions caused by CEX facility effects. Although increased background pressure increased the central core current density, the residuals indicate the angular location of ion migration from the central core within ±10° is largely unaffected by downstream distance.

The slope of the extrapolated collected ion current density in Fig. 11 provides information about the angular location of increased current density due to neutral ingestion and dispersion from beam scattering due to CEX collisions with facility neutrals. The slope appears to be dominated by two distinct effects in the plume. These two effects are each modeled with a Gaussian distribution, and the modeled slope distribution is the superposition of these Gaussian best-fit curves. The choice of a Gaussian distribution is arbitrary, but may be appropriate for processes related to the thermalized facility neutral propellant population. The two fitted Gaussian curves, the modeled slope, and the experimental slope are compared in Fig. 12 at 8 to 20 CCDD. The superposition of Gaussian

distributions shows consistent agreement with the experimental distribution of slope for all downstream distances. Although the Gaussian distribution may not be the correct physical distribution, this analysis provides a qualitative characterization of the angular range and relative magnitude of facility effects in the plume.

The first effect leads to a positive increase in the slope about thruster centerline, and is attributed to ionization and acceleration of ingested facility neutrals. The magnitude of the positive slope in the central core decreased with downstream distance as approximately R^2, and affected a slightly larger angular range of the plume as downstream

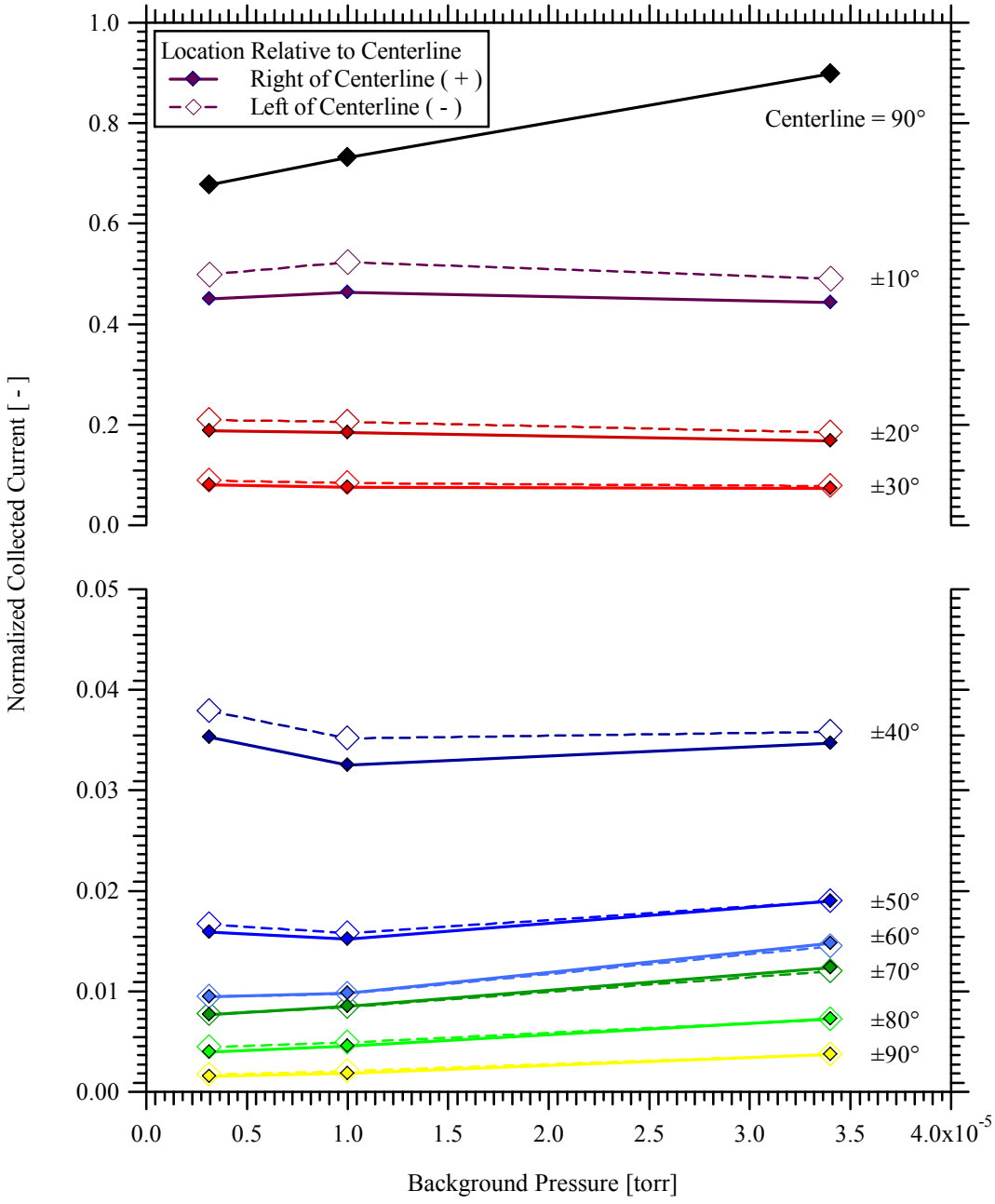

Figure 10. Normalized collected ion current of Configuration 1 as a function of background pressure at discrete angular locations in the plume at 20 CCDD. Measurements are normalized to the maximum collected current of the profile at 3.4×10^{-5} torr.

distance increased. The decrease in slope is the result of CEX collisions with facility neutrals downstream of the primary acceleration zone, which results in a secondary population of low energy ions and dispersion of the primary ion beam. CEX processes with facility neutrals within the discharge channel may also lead to increased current density in the central core, but would not increase ion beam current or discharge current. Facility neutrals may also undergo direct electron-impact ionization in the far-field region, and will cause a net increase in the collected ion current.

The second effect is broader and leads to a negative slope in the central core about thruster centerline. This is believed to be the result of CEX collisions with facility neutrals near the thruster exit downstream of the primary acceleration zone. In this case, no additional current is created and the primary ion beam is dispersed. The outer edge of this distribution corresponds to the location of minimum residuals at each operating condition. The width of the Gaussian attributed to downstream CEX collisions with facility neutrals was relatively constant with downstream distance in the far-field. The residuals decline where the effects of ionization and acceleration of facility neutrals are approximately equal to the effects of CEX collisions with facility neutrals near the thruster exit.

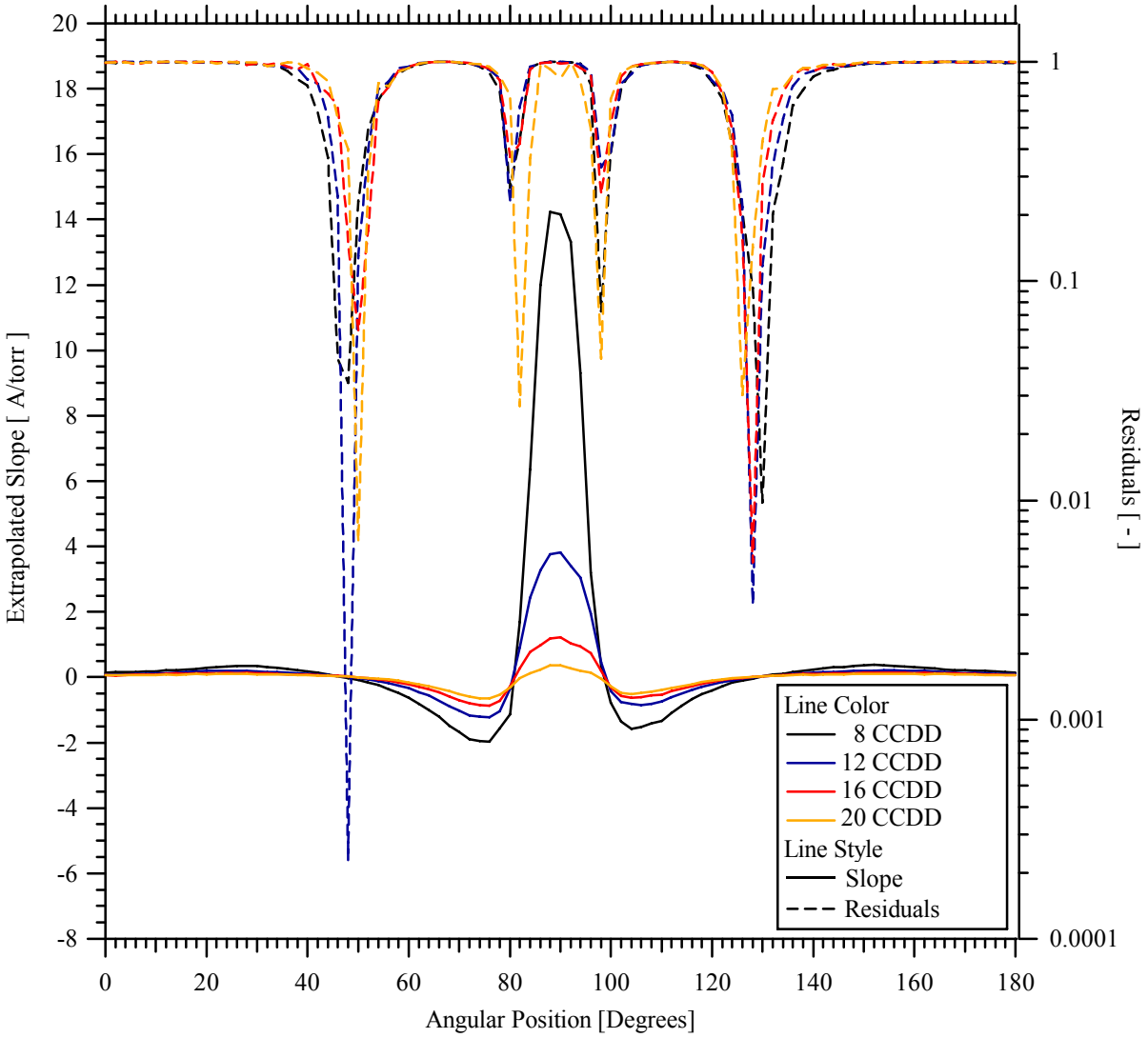

Figure 11. Residuals and slope of the extrapolated collected ion current of the nested Faraday probe Configuration 1 as a function of angular position at 8, 12, 16, and 20 CCDD.

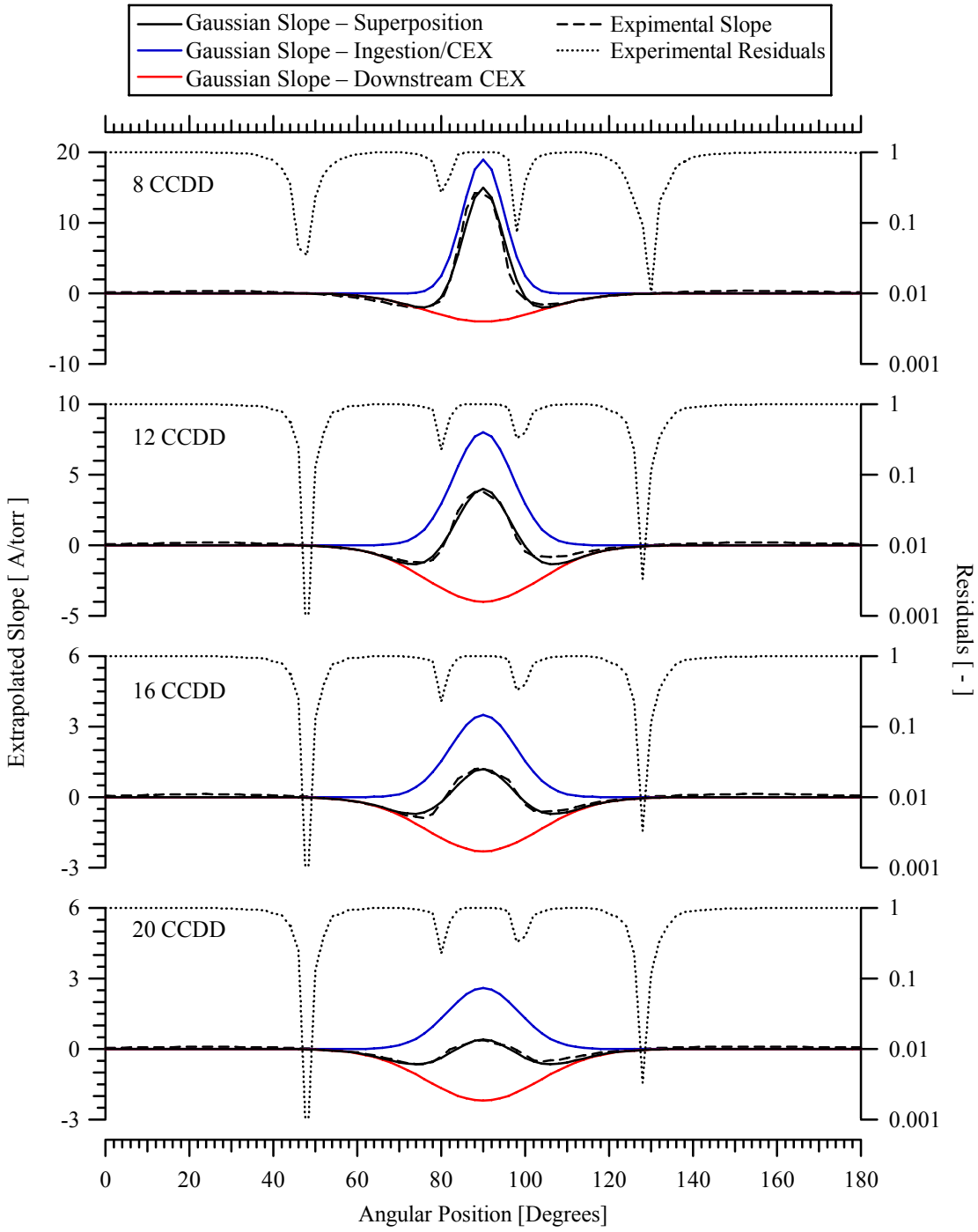

Figure 12. Residuals and slope of the extrapolated collected ion current of the nested Faraday probe Configuration 1 as a function of angular position at 8, 12, 16, and 20 CCDD. A superposition of two Gaussian curves is fit to the experimental slope.

The complete effects of background pressure on current density profiles are shown in Fig. 13. These profiles show the escalation of ion current density in the central core with increased background pressure, which was attributed to ionization of ingested neutrals upstream of the primary acceleration region. Increased current density on the wings is primarily the result of ambient low energy facility ions and beam ion scattering from the central core due to CEX collisions.

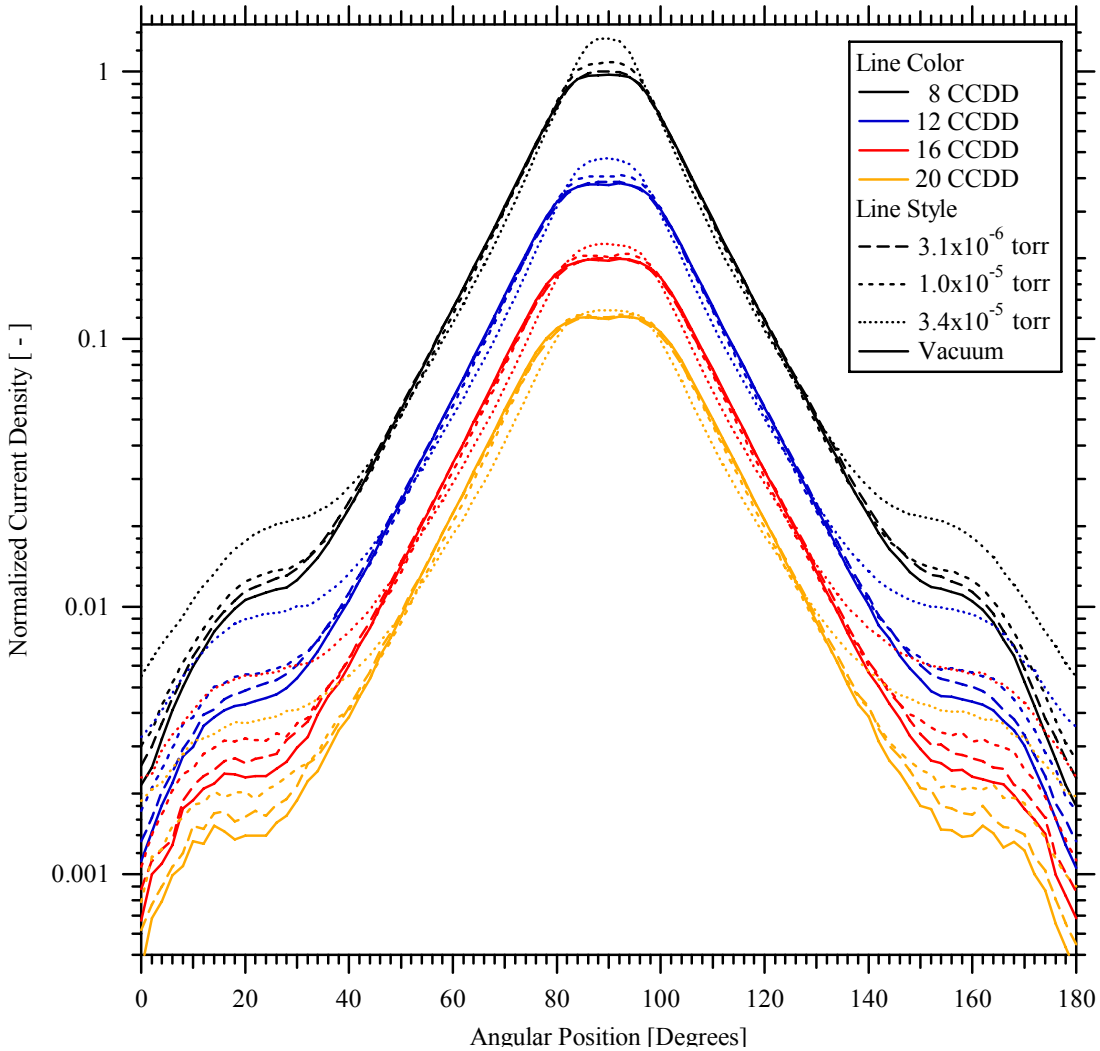

Figure 13. Normalized ion current density profiles of the nested Faraday probe Configuration 1 as a function of angular position at 8, 12, 16, and 20 CCDD. The extrapolated vacuum profiles are compared to measurements at background pressures of 3.1×10^{-6}, 1.0×10^{-5}, and 3.4×10^{-5} torr. Current density profiles are normalized to the maximum extrapolated vacuum current density at 8 CCDD.

Current density profiles of the four nested Faraday probe configurations are extrapolated to vacuum conditions for all downstream distances in Fig. 14. These vacuum current density profiles isolate facility effects, and provide insight into the ion migration that would be present on-orbit. The configurations exhibit consistent profiles at all distances, and further increase confidence in the methods developed for determination of on-orbit current density. The current density of Configuration 1 is slightly larger than the other configurations, and is attributed to measurement and/or alignment error of the inner collector. This increased current density profile manifests as a ~5% increase in the integrated ion beam current compared to the other configurations. The current utilization, equivalent to the ion beam current relative to the total thruster discharge current, is listed in Table 2 for vacuum

conditions of all probe configurations at all downstream distances. Configurations 2, 3, and 4 are within a 0.03 range of current utilization for all downstream distances, and the magnitudes of ion beam current relative to discharge current are consistent with expected values from Hall thruster performance models.

Table 2. Ratio of integrated ion beam current to thruster discharge current at vacuum conditions for nested Faraday probe Configurations 1 to 4 at 8, 12, 16, and 20 CCDD.

Downstream Distance [CCDD]	I_{Beam}/I_d			
	Configuration 1	Configuration 2	Configuration 3	Configuration 4
8	0.88	0.82	0.81	0.80
12	0.89	0.84	0.82	0.81
16	0.90	0.84	0.82	0.82
20	0.90	0.85	0.82	0.83

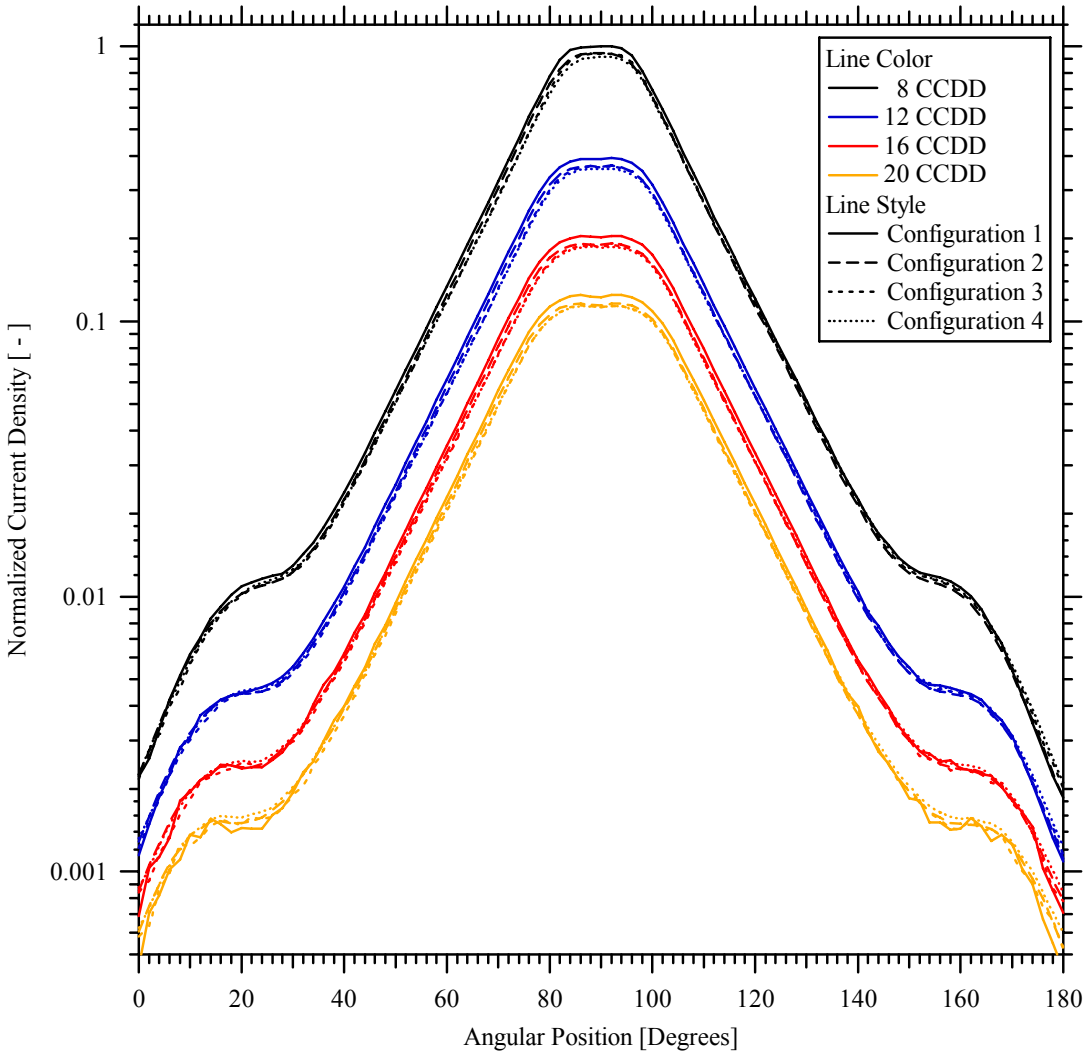

Figure 14. Normalized ion current density profiles at vacuum conditions of the nested Faraday probe Configurations 1, 2, 3, and 4 as a function of angular position at 8, 12, 16, and 20 CCDD. Current density profiles are normalized to the maximum extrapolated vacuum current density of Configuration 1 at 8 CCDD.

VI. Calculation of Beam Divergence

To accurately assess plume divergence, it is necessary to characterize the migration of primary beam ions in the plume due to external fields and CEX collisions with anode and cathode neutrals. Although this scattering would be present on-orbit, beam divergence downstream of the primary ion acceleration zone where thrust is produced will cause an over-prediction of plume divergence losses in the Hall thruster efficiency.

Jet momentum losses due to beam divergence are naturally expressed as a momentum-weighted average cosine.[14] Charge divergence in the plume is indicative of the loss in thrust due to off-axis ion velocity, and is often used as an alternative for experimental characterization of performance losses due to plume divergence. The momentum-weighted average divergence is approximated as the charge-weighted average divergence in Eq. (9) for an axisymmetric plume.

$$<\cos(\theta)>_{mv} \cong \frac{2\pi R^2 \int_0^{\pi/2} J[\theta]\cos(\theta)\sin(\theta)\,d\theta}{2\pi R^2 \int_0^{\pi/2} J[\theta]\,\sin(\theta)\,d\theta} = <\cos(\theta)>_J \tag{9}$$

An effective plume divergence angle, λ, may be calculated as shown in Eq. (10). This angle is significantly less than the 95% divergence half-angle that is typically reported for evaluation of plume expansion.

$$\lambda = \cos^{-1}\left(<\cos(\theta)>_J\right) = \cos^{-1}\left(\frac{I_{Axial}}{I_{Beam}}\right) \tag{10}$$

The axial component of ion beam current from the far-field current density distributions shown in Fig. 14 will be studied relative to the angle from channel centerline, as opposed to thruster centerline. Fig. 15 illustrates the reduction in plume divergence half-angle with respect to channel centerline, α_A, compared to the plume divergence

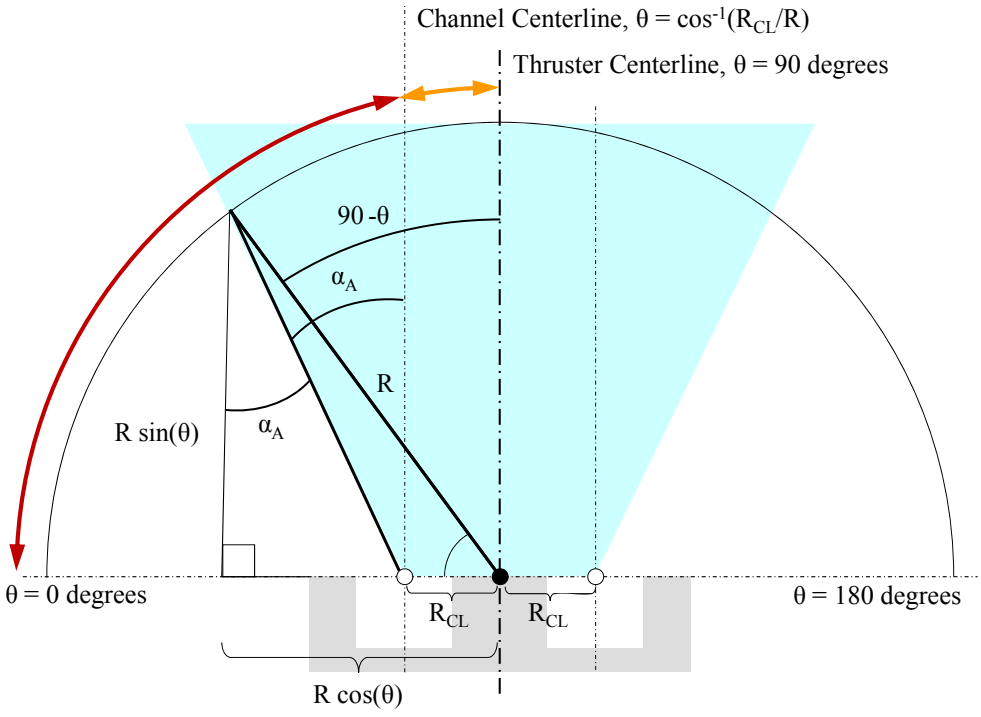

Figure 15. Diagram of the axial component of beam current relative to channel centerline.

angle with respect to thruster centerline, 90°-θ. The reference frame based on channel centerline reduces systematic error in plume divergence associated with beam ions in the central core, and is similar to the methodology developed in Section IV.B to reduce the systematic error of a point source measurement coordinate system.

The axial component of ion beam current is calculated in Eq. (11) with respect to channel centerline using α_A, and includes the correction factors developed in Sections IV.A and IV.B.

$$I_{Axial} = 2\pi R^2 \int_0^{\pi/2} \frac{I[\theta]\cos\left(\alpha_A[\theta, R, R_{CL}]\right)}{A_C + \kappa_G}\left(\frac{\kappa_D[\theta]}{\kappa_A[\theta]}\right)\sin(\theta)d\theta \tag{11}$$

In Fig. 15, the cosine loss in beam current is fixed at α_A=0° in the central core and calculated with respect to channel centerline in the region beyond the central core to θ=90°. This piecewise function for α_A is expressed in Eq. (12).

$$\alpha_A[\theta, R, R_{CL}] = \begin{cases} \tan^{-1}\left(\dfrac{\cos(\theta) - \dfrac{R_{CL}}{R}}{\sin(\theta)}\right) & \text{for} \quad 0^\circ \le \theta \le \cos^{-1}\left(\dfrac{R_{CL}}{R}\right) \\ 0 & \text{for} \quad \cos^{-1}\left(\dfrac{R_{CL}}{R}\right) \le \theta \le 90^\circ \end{cases} \tag{12}$$

The ratio of the axial component of ion beam current calculated in Eq. (11) relative to the total ion beam current determined from Eq. (8) is shown for all background pressures and all configurations of the nested Faraday probe in Fig. 16. As downstream distance increases, the ratio decreases for all cases. This effect is expected and is primarily attributed to divergence caused by the external potential field structure, CEX collisions with anode and cathode neutrals, and CEX collisions with facility neutrals for the profiles at finite background pressure.

The ratios of the axial component of ion beam current relative to the total ion beam current in Fig. 16 are extrapolated as a 2nd order polynomial trend to the exit plane to more accurately assess the loss of divergence on thrust. While additional ion acceleration may occur downstream of the of the discharge channel exit plane, a majority of the thrust has been generated within one thruster diameter. Sixteen trendlines of I_{Axial}/I_{Beam} as a function of downstream distance correspond to the four probe configurations at four facility background pressures, including vacuum. All of the second order polynomial trendlines intersect at the exit plane value of ~0.94±0.01 for this thruster operating condition. This excellent agreement of four probe configurations over a wide range of facility background pressures and downstream distances indicates a high degree of accuracy and precision.

It should be noted that the ratio of I_{Axial}/I_{Beam} extrapolated to vacuum conditions showed a significant decline with downstream distance, albeit less than the reduction with increased facility background pressure. This reveals that a significant source of plume divergence is unrelated to facility effects. Based on these measurements, the ratio of I_{Axial}/I_{Beam} may diminish by more than 5% in the near-field plume before reaching a steady value in the far-field plume.

The coefficients of the 2nd order polynomial trendlines varied with background pressure. Further investigations also showed variations in the 2nd order polynomial coefficients with thruster operating conditions, although the excellent fit to a 2nd order polynomial was consistent. No universal function was found that correlated these coefficients to background pressure, discharge voltage, and mass flow rate. For a general 2nd order polynomial of the form $y(x)=A_2x^2+A_1x+A_0$, increased background pressure increased the coefficient A_1 and decreased the coefficient A_2. In this form, the coefficient A_0 is the ratio of the axial component of ion beam current relative to the total ion beam current at vacuum conditions.

Variations in the polynomial coefficients with discharge voltage and anode mass flow rate are more difficult to isolate and quantify due to the dependence on plume focusing and the location of ionization. Initial results indicate higher discharge voltage decreased the magnitude of both coefficients. This relationship is attributed to the more collimated beam that is typically seen during high-voltage operation.

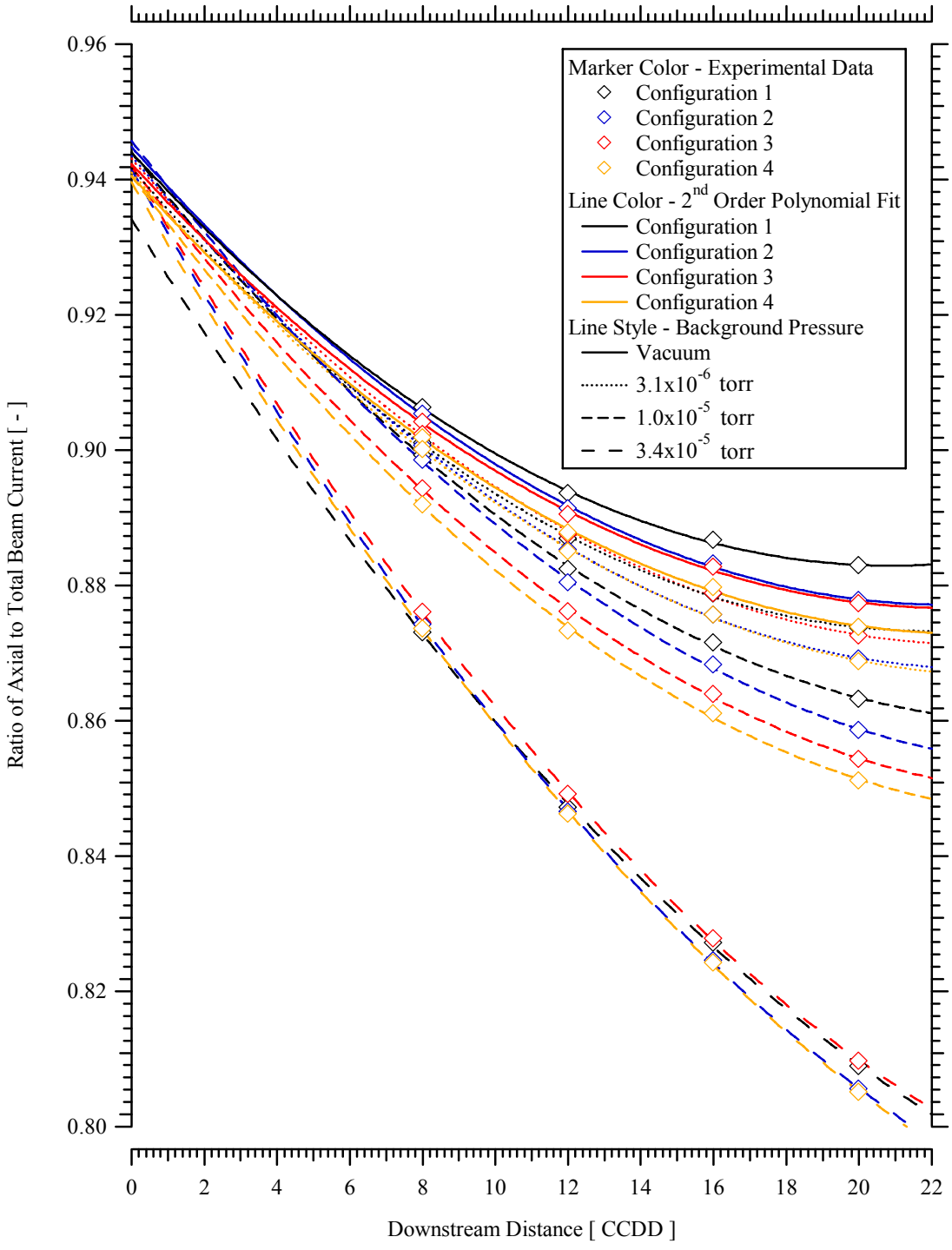

Figure 16. Experimental data (markers) and 2nd order polynomial trendlines (lines) of the ratio of the axial component of ion beam current relative to the total ion beam current of the nested Faraday probe Configurations 1, 2, 3, and 4 as a function of downstream distance at background pressures of 3.1×10^{-6} torr, 1.0×10^{-5} torr, 3.4×10^{-5} torr, and the ratio extrapolated to vacuum. Experimental data deviates from the trendlines by less than ±0.1%.

The anode mass flow rate is believed to have two competing effects on divergence. Increased propellant flow rate corresponds to a narrower axial region of ionization and acceleration in the discharge, along with a more concentrated ion density near channel centerline.[15] These effects lead to a decrease in divergence due to enhanced plume focusing, and would likely have a similar effect as discharge voltage on the polynomial coefficients. However, the increased neutral flow may also lead to increased CEX collisions with thruster neutrals downstream of the exit plane, thereby increasing ion scattering in the far-field plume. A simple analytical model is deemed insufficient to fully characterize the influence of beam focusing and facility effects on plume divergence. Additional systematic investigations and numerical simulations with a high fidelity source model are required to determine these relationships.

VII. Recommendations for High Accuracy Current Density Measurements

Based on the experimental results in this investigation, the best approach for high accuracy current density distributions is to characterize the plume with variations in facility background pressure and downstream distance. The analytical methods and experimental techniques described in this paper may be used to determine Hall thruster current density profiles and integrated ion beam current to a high degree of accuracy. In order to minimize uncertainty of far-field Faraday probe measurements, the following guidelines are recommended for Faraday probe design, experimental approach, and analysis of results. Several of these guidelines are conventional practice or have been recommended in previous literature.[3,11]

1. Account for ions collected in the gap volume by increasing the effective ion collection area with κ_G. Consider effects introduced by ion collection at the base of the gap volume when selecting a Faraday probe design. A ceramic base is recommended for investigations at variable or high background pressure.[12]
2. Select a Faraday probe design with a 5 to 10 Debye length gap for a wide range of downstream distances and pressures. Select collector and guard ring material with minimal SEE coefficient, such as molybdenum, graphite, or tungsten.
3. Conduct Faraday probe current density measurements at a minimum of 3 facility background pressures to determine the vacuum current density profiles. The background pressures should range by at least one order of magnitude.
4. Conduct Faraday probe current density measurements at a minimum of 3 downstream distances to determine the axial component of ion beam current at the exit plane. For far-field measurements about a single axis of rotation using a spherical measurement coordinate system, the distance should be greater than 4 CCDD. For near-field measurements based on a cylindrical measurement coordinate system, spatial effects and cosine losses should be estimated and the maximum distance should be less than approximately one thruster diameter downstream using a dynamic window integration method[15] or similar technique.
5. Include the correction factors κ_A, κ_D and α_A to account for the point source measurement coordinate geometry and the annular thruster geometry.

The guidelines provide a framework for determination of on-orbit current density profiles and minimize experimental measurement uncertainty. Following the recommendations in these guidelines is expected to minimize uncertainty in the total ion beam current to ±3% and the uncertainty in the axial component of ion beam current to ±5%. Ideally, the experimental current density profiles extrapolated to vacuum will enable comparison with numerical simulations in the absence of facility effects, thereby reducing the computational complexity and time.

Near-field measurements would seem to minimize the uncertainty associated with far-field measurements. However, these measurements introduce new difficulties, including perturbation of the plasma discharge, a wider range of Debye length in the measurement domain, and possibly SEE effects from the probe collector. In addition, ingestion and near-field CEX collisions with facility neutrals are expected to affect near-field measurements. Thus, the ion current density profiles should still be characterized for variations in distance and background pressure. A second set of spatial corrections for measurement geometry may also be necessary to reduce systematic error associated with cylindrical integration as distance from the exit plane increases.

VIII. Summary and Conclusions

A comprehensive investigation of nude Faraday probe design and analysis techniques was conducted with the AFRL nested Faraday probe. Correction factors accounting for variations in distance and angle of the Faraday probe collector surface to the ion beam were introduced through a theoretical analysis of the near-field plume with the Hall thruster modeled as two point sources. A gap correction factor was utilized to adjust the effective probe collection area for ions collected by the walls in the gap volume. These correction factors and methods for evaluating plume properties minimized systematic measurement error and facility effects on current density distributions. The corrected plume properties are in line with expected values of ion beam current based on Hall thruster performance and discharge properties. Precision in total ion beam current measurements was within a 3% range for all nested Faraday probe configurations at all distances.

Facility effects in this investigation were studied over a range of downstream measurement distances and background pressures for all nested Faraday probe configurations. The measured current density at each angular location in the plume was extrapolated to vacuum conditions, similar to past studies by Azziz[11] and deGrys[8]. Ion migration in the plume due to facility effects was studied and compared to plume expansion of the extrapolated vacuum current density profiles. This approach enabled a more accurate description of the on-orbit current density profiles using ground measurements. Variations in the ion current density with facility background pressure were studied as the superposition of two Gaussian curves. These curves provided qualitative information about the ionization of ingested neutrals and CEX collisions of facility neutrals in the near-field plume.

The ratio of the axial component of ion beam current with respect to the total ion beam current was extrapolated with a 2nd order polynomial to the thruster exit plane. Coefficients of the 2nd order polynomial fit varied with background pressure, thruster discharge voltage, and mass flow rate. This methodology resulted in consistent agreement to within 1% for all background pressures and probe configurations, and led to a more accurate evaluation of plume divergence losses in thruster efficiency. For the low-power Hall thruster ion source in this investigation, the axial component of ion beam current at vacuum conditions decreased by approximately 5% to 10% from the exit plane to the far-field plume. This was attributed to CEX collisions with thruster neutrals and divergence by the external potential field structure. Although ion beam current may be accurately estimated in the far-field plume, the axial component of ion beam current requires additional investigation to accurately assess the loss of thrust due to ion beam divergence. This recommendation applies to near-field measurements as well, since these measurements introduce complications associated with perturbation of the discharge, a reduction in the Debye length, and possibly SEE effects. In addition, ingestion and near-field CEX collisions with facility neutrals are expected to affect near-field measurements. Thus, characterization of ion current density profiles with variations in distance and background pressure are advised.

Based on the results of this systematic investigation, the measurement uncertainty of Faraday probe ion beam current measurements is estimated as ±3% and the uncertainty in the axial component of ion beam current is estimated as ±5% when the recommendations in Section VII are followed. The reductions in measurement uncertainty and the increased capability to approximate on-orbit plume expansion are a significant improvement for comparisons with numerical simulations and analysis of Hall thruster performance.

References

[1] Boyd, I. D., "Review of Hall Thruster Plume Modeling," *Journal of Spacecraft and Rockets*, Vol. 38, No. 3, 2001, pp. 381-387.

[2] Manzella, D. H., Sankovic, J. M., "Hall Thruster Ion Beam Characterization," AIAA Paper 95-2666, 1995, (also NASA TM-107034).

[3] Walker, M. L. R., Hofer, R. R., Gallimore, A. D., "Ion Collection in Hall Thruster Plumes," *Journal of Propulsion and Power*, Vol. 22, No. 1, 2006, pp. 205-209.

[4] Walker, M. L. R., Hofer, R. R., Gallimore, A. D., "The Effects of Nude Faraday Probe Design and Vacuum Facility Backpressure on the Measured Ion Current Density Profile of Hall Thruster Plumes," AIAA Paper 2002-4253, 2002.

[5] Hargus Jr., W. A., Fife, J. M., Mason, L., Jankovsky, R. S., Haag, T. W., Pinero, S., "Preliminary Performance Results of the High Performance Hall System SPT-140," AIAA Paper 2000-3250, 2000.

[6] Walker, M.L.R., Victor, A.L., Hofer, R.R., Gallimore, A.D., "Effect of Backpressure on Ion Current Density Measurements in Hall Thruster Plumes," *Journal of Propulsion and Power*, Vol. 21, No. 3, May-June 2005.

[7] Boerner, J. J., "Computational Simulation of Faraday Probe Measurements," Doctoral Dissertation, Department of Aerospace Engineering, University of Michigan, Ann Arbor, MI, 2008.

[8] de Grys, K.H., Tilley, D.L., Aadland, R.S., "BPT Hall Thruster Plume Characteristics," AIAA Paper 99-2283, 1999.

[9] Hofer, R. R., Walker, M. L. R., Gallimore, A. D., "A Comparison of Nude and Collimated Faraday Probes for Use with Hall Thrusters," IEPC-01-020, 2001.

[10] Rovey, J.L., Walker, M.L.R., Gallimore, A.D., Peterson, P.Y., "Evaluation of a Magnetically-Filtered Faraday Probe for Measuring the Ion Current Density Profile of a Hall Thruster," AIAA Paper 2004-3948, 2004.

[11] Azziz, Y., "Experimental and Theoretical Characterization of a Hall Thruster Plume," Doctoral Dissertation, Department of Aeronautics and Astronautics, Massachusetts Institute of Technology, Cambridge, MA, 2007.

[12] Brown, D. L., "Investigation of Low Discharge Voltage Hall Thruster Characteristics and Evaluation of Loss Mechanisms," Doctoral Dissertation, Department of Aerospace Engineering, University of Michigan, Ann Arbor, MI, 2009.

[13] King, L. B., Gallimore, A. D., Marrese, C. M., "Transport-Property Measurements in the Plume of an SPT-100 Hall Thruster," *Journal of Propulsion and Power*, Vol. 14, No. 3, 1998, pp. 327-335.

[14] Brown, D. L., Larson, C. W., Beal, B. E., Gallimore, A. D., "Methodology and Historical Perspective of a Hall Thruster Efficiency Analysis," *Journal of Propulsion and Power*, (Accepted for Publication Aug. 2009).

[15] Reid, B. M., "The Influence of Neutral Flow Rate in the Operation of Hall Thrusters," Doctoral Dissertation, Department of Aerospace Engineering, University of Michigan, Ann Arbor, Michigan, 2009.